Tellus (2007), 59B, 372–380
Printed in Singapore. All rights reserved

TELLUS

Simulation of nitrate aerosol concentrations over East Asia with the model system RAMS-CMAQ

By MEIGEN ZHANG[1]*, LIJIE GAO[1,3], CUI GE[1,3] and YOUPING XU[2,3], [1]*State Key Laboratory of Atmospheric Boundary Layer Physics and Atmospheric Chemistry, Institute of Atmospheric Physics, Chinese Academy of Sciences, Beijing 100029, China;* [2]*Beijing Institute of Applied Meteorology, Beijing 100029, China;* [3]*Graduate School of the Chinese Academy of Sicences, Beijing 100049, China*

(Manuscript received 25 April 2006; in final form 1 November 2006)

ABSTRACT

The Models-3 Community Multi-scale Air Quality modeling system (CMAQ) coupled with the Regional Atmospheric Modeling System (RAMS) is used to analyse the geographical and the seasonal characteristics of nitrate aerosol (ANO_3) concentration distributions over East Asia. Three-dimensional concentrations in January, March, April, July and October of 2001 are simulated, and for the evaluation of model performances, the simulated values of wind direction, wind speed, temperature, specific humidity, nitric oxide (NO), nitrogen oxide (NO_2), ANO_3 and ammonium aerosol (ANH_4) are compared with the observational data obtained onboard the P-3B aircraft during its four consecutive flights over the South China Sea, the East China Sea, the Yellow Sea and the water areas to the east of Japan conducted on 13, 17, 18 and 21 March 2001. The observed data are 5-min averaged and the model results with a 1-hour temporal resolution are interpolated to the aircraft location and time using trilinear interpolation. Comparison shows that the observed values exhibit strong temporo-spatial variations, and the model reproduces these variations reasonably well. The simulated values of wind direction, wind speed, temperature and specific humidity are generally in good agreement with the observed ones, their correlation coefficients reach 0.66, 0.94, 0.99 and 0.96, respectively. Comparison also shows that the average mixing ratios of modelled and observed NO, NO_2, ANO_3 and ANH_4 agree reasonably well with each other, the correlation coefficient for ANO_3 and ANH_4 are larger than 0.8, but the simulated standard deviations are smaller than the observed one, and the correlation coefficient for NO and NO_2 are 0.48 and 0.44.

Analysis of horizontal distributions of monthly averaged ANO_3 concentrations in the boundary layer indicates that the ANO_3 mixing ratios have noticeable differences among the four seasons. Generally the concentrations are high in the winter, spring and fall and low in the summer, and seasonal variations are typically strongest over China and Japan. Highest concentrations are found over eastern China where emissions of nitrogen oxides and ammonia are high and long-range transport may cause elevated concentrations in remote areas under favourable meteorological conditions, but the seasonal variation in the ANO_3 concentrations is heavily influenced by the changes in precipitation and temperature.

1. Introduction

Nitrate aerosols (ANO_3) are secondary aerosols produced from nitrogen oxides ($NOx = NO + NO_2$), and play an important role in many environmental issues as climate changes, acid rain and smog. A recent critical assessment of nitrate observations in Europe showed that nitrate significantly contributed to the aerosol concentration in Northern Europe, especially in winter (October–March), large contributions of nitrate to the total aerosol mass were found in the western Europe, where nitrate concentrations often exceeded those of sulphate (ASO_4) (Schaap et al., 2002). In the United Kingdom ANO_3 concentrations were reported to have a southeast to north-west gradient, and its annual average levels in the south-east region were generally higher than those of ASO_4 (AQEG, 2005; Turnbull and Harrison, 2000). While in East Asia, a region of the world with large and rapidly increasing anthropogenic emissions, the NOx emissions have increased by 58% from 1975 (2.05 TgN/yr) to 1987 (3.25 TgN/yr) (Kato and Akimoto, 1992), and van Aardenne et al. (1999) predicted an increase of almost fourfold in NO_x emissions from 1999 to 2020. Especially in China anthropogenic emissions associated with fossil fuel burning have grown significantly as there experienced a period of rapid economic development and industrial expansion in the last three decades (e.g., Streets and Waldhoff, 2000). Many observations indicate that the increase in NOx emissions is exacerbating the acid rain problem in East

*Corresponding author.
e-mail: mgzhang@mail.iap.ac.cn
DOI: 10.1111/j.1600-0889.2007.00255.x

Asia (e.g., Kim and Cho, 2003), especially in China (e.g., Xie, 2002; Yu et al., 2003). Xie (2002) reported that nitrate ion was steadily increasing in the rain water collected in Guangzhou in southern China in the period of 1996 to 2000.

At present our knowledge of aerosol distributions and associated effects on air quality and climate changes is largely dependent on models (IPCC, 2001). There are few observational data from remote locations against which such models can be tested, especially over the oceans (IPCC, 2001). Such data are especially critical in areas impacted by transport from regions with rapidly developing economies where emission controls are often minimal and emission rates poorly documented. So although nitrate aerosols were often included in the calculations of regional-scale chemical transport models applied to East Asia (e.g., Zhang et al., 2004; Han et al., 2005), their temporo-spatial distributions are still poorly characterized over the region.

In the period from 4 March to 2 April 2001, the Transport and Chemical Evolution over the Pacific (TRACE-P) field campaign (Jacob et al., 2003) was conducted with two NASA aircrafts (DC-8 and P-3B) over the western Pacific along the Asian Pacific Rim. The aircrafts DC-8 and P-3B performed 11 and 12 observations, respectively, with bases near Hong Kong, Okinawa and Tokyo, and each flight lasted about 9 hours. These flights are named as DC-8 07 to 17 and P-3B 08 to 19. These airborne observations obtained an extensive suite of meteorological parameters, trace gases and aerosols. This study is to take advantage of this observational data set to examine regional-scale performances of a comprehensive chemistry-transport model system (Zhang et al., 2004) and then to investigate geographical and seasonal characteristics of nitrate aerosol concentration distributions over East Asia.

This paper is divided into four sections. We briefly describe the model, its initial and boundary conditions in section 2. In section 3, we firstly compare model results with the observations from the TRACE-P missions, and then discuss geographysical and seasonal distributions of nitrate aerosol concentrations over East Asia. Conclusions are presented in section 4.

2. Model system and input parameters

The model system used in this study has two major components - the Models-3 Community Multi-scale Air Quality (CMAQ) modeling system (Byun and Ching, 1999) and the Regional Atmospheric Modeling System (RAMS; Pielke et al., 1992). CMAQ is an Eulerian-type model and it simulates concurrently the atmospheric and land processes affecting the transport, transformation and deposition of air pollutants and their precursors on both regional and urban scales. While RAMS is a highly versatile numerical code for simulating and forecasting meteorological phenomena. In this study it is used to produce regional scale meteorological fields including boundary layer turbulence, cloud and precipitation necessary for the CMAQ calculation. CMAQ coupled with RAMS has recently been successfully applied to East Asia to simulate tropospheric ozone and sulphur dioxide (Zhang et al., 2003, 2004)

In this study CMAQ is configured with the chemical mechanism of the Regional Acid Deposition Model version 2 (RADM2; Stockwell et al., 1990), including gas-phase and aqueous reactions leading to secondary aerosol formation, and extended to include aerosol processes on the basis of the Regional Particulate Model (RPM; Binkowski and Shankar, 1995). In the extended RADM2 the particle size distribution is represented as the superposition of three lognormal subdistributions, and the processes of coagulation and particle growth by the addition of new mass, particle formation, etc. The reaction of nitrogen pentoxide (N_2O_5) on aerosol surface is a source for nitric acid during night-time, whereas during the day the nitrogen trioxide radical is readily photolysed. This reaction is parameterized following Dentener and Crutzen (1993). The thermodynamic equilibrium between gaseous nitric acid (HNO_3), ammonia (NH_3) and particulate ammonium nitrate (NH_4NO_3) and ammonium sulphate and aerosol water is considered (Kim et al., 1993): the ammonia deficient regime (in which the ionic ratio of ammonium to total sulphate ion is less than two) leads to an acidic aerosol system with very low concentrations of dissolved nitrate ion which depend very strongly on ambient relative humidity; the second regime is one in which the ammonium to sulphate ratio exceeds two, the sulphate is completely neutralized, and there is excess ammonia. If there is nitric acid vapour in the system, it will dissolve in the aqueous particles along with the excess ammonia and produce abundant nitrate. For the cases when the relative humidity is low that the aerosol liquid water content comprises less than 20 percent of the total aerosol mass, and the ionic ratio of ammonium to sulphate is greater than two, the appearance of "dry ammonium nitrate" aerosol is calculated from the following equilibrium relationship (Mozurkewish, 1993):

$$NH_4NO_3 \Leftrightarrow NH_3 + HNO_3. \qquad 2.$$

For the CMAQ inputs, emissions of nitrogen oxides, sulphur dioxide, carbon monoxide, non-methane hydrocarbon species and ammonia from anthropogenic activities and open biomass burning were obtained from the $0.5^\circ \times 0.5^\circ$ monthly inventory (Streets et al., 2003). Nitrogen oxides and ammonia from soil were adopted from the Global Emissions Inventory Activity (GEIA) $1^\circ \times 1^\circ$ monthly global inventory (Benkovitz et al., 1996). Aircraft emissions were based on the Emission Database for Global Atmospheric Research (EDGAR; Olivier et al., 1996). Sulphur dioxide emissions arising from volcanoes were based on the estimates by Streets et al. (2003). These different emission inventories are preprocessed to form a unified one with the same spatial resolution of CMAQ for the simulation.

In this study RAMS was exercised in a four-dimensional data assimilation mode using analysis nudging with re-initialization every four days, leaving the first 24 hours as the initialization period. The three-dimensional meteorological fields for RAMS were obtained from the European Center for Medium-Range

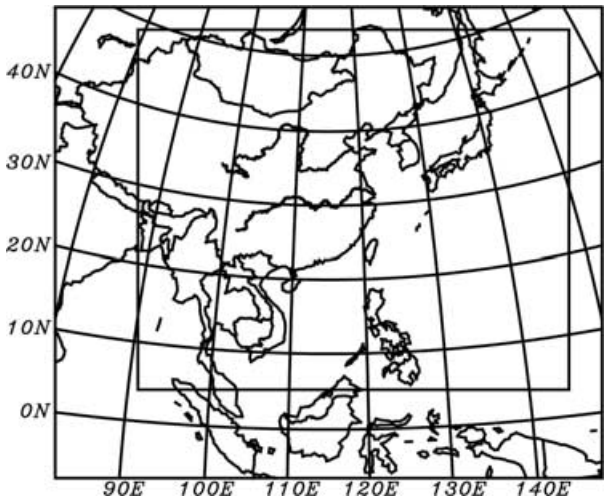

Fig. 1. Model domain for RAMS (outer region) and CMAQ (inside region) used in this study.

Weather Forecasts (ECMWF) analyzed data sets with $1^\circ \times 1^\circ$ resolution and with six-hour interval. Sea Surface Temperatures (SST) for RAMS were based on weekly mean values and observed monthly snow-cover information as the boundary conditions for the RAMS calculation.

The model domain (shown in Fig. 1) is $8000 \times 5600\,\mathrm{km}^2$ (outside region) for RAMS and $6240 \times 5440\,\mathrm{km}^2$ (inside region) for CMAQ on a rotated polar-stereographic map projection centred at (25°N, 115°E) with 80 km mesh. RAMS and CMAQ have the same model height. For RAMS there are 23 vertical layers in the σ_z coordinates system unequally spaced from the ground to ~23 km, with about 9 layers concentrated in the lowest 2 km of the atmosphere in order to resolve the planetary boundary layer, while there are 14 levels for CMAQ with the lowest 7 layers being the same as those in RAMS.

Initial and boundary conditions of chemical species in CMAQ were chosen to reflect the East Asian situation. Recent measurements were used whenever possible. To evaluate the impact of the anthropogenic emissions on the distributions of trace gases and aerosols, the initial and boundary conditions were generally chosen at the lower end of their observed range (e.g., the northern and western boundary conditions for O_3, NO_2, ANO_3 and ASO_4 were 30 ppbv, 0.2 ppbv, 0.5 $\mu g/m^{-3}$ and 1 $\mu g/m^{-3}$, respectively) so as to allow the emissions and chemical reactions to bring them closer to their actual values during the initialization period (Zhang et al., 2003).

3. Results and discussion

3.1. Model evaluation

With the model system described in the previous section, meteorological fields and three-dimensional concentrations of trace gases and aerosols over East Asia in the periods of 26 December 2000 to 31 January, 22 February to 5 May, 25 June to 31 July and 25 September to 31 October of 2001 are simulated. Zhang et al. (2006) compared simulated concentrations of ozone and its related species with observations obtained during the TRACE-P experiment and comparison indicates that the model system reproduced the tempo-spatial distributions of ozone and related species reasonably well and most model results were within a factor of two of the observations. During the period of 4 March to 2 April, two aircrafts DC-8 and P-3B conducted 11 (DC-8 flights 07 to 17) and 12 (P-3B flights 08 to 19) observations, respectively, over a broad area covering Hong Kong, Okinawa, the East China Sea, the Yellow Sea and the water areas to the south and the east of Japan with bases near Hong Kong, Okinawa and Tokyo, and each flight lasted more than 8 hours (Jacob et al., 2003). In this study, four consecutive P-3B flights 12 to 15 were selected to evaluate the model performances. Their horizontal flight tracks are presented in Fig. 2. These flights were performed on 13, 17, 18 and 21 March, respectively, over four different areas: the South China Sea, the East China Sea, the Yellow Sea and the water areas to the east of Japan. Comparison with these specific flights is to test the model's ability to produce three-dimensional distributions of meteorological parameters and chemical species in more detail. For these comparisons the 5-min merged data set for the P-3B was used, and the model results with a 1-hour temporal resolution were interpolated to the aircraft location and time using trilinear interpolation.

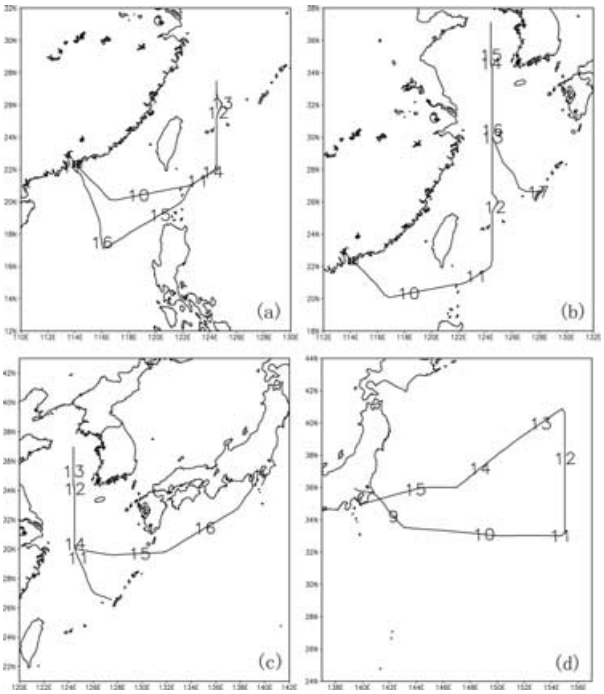

Fig. 2. Horizontal tracks of the P-3B flights 12 to 15 conducted on (a) 13 March, (b) 17 March, (c) 18 March, and (d) 21 March, respectively. Numbers are flight time in the Chinese Standard Time (CST).

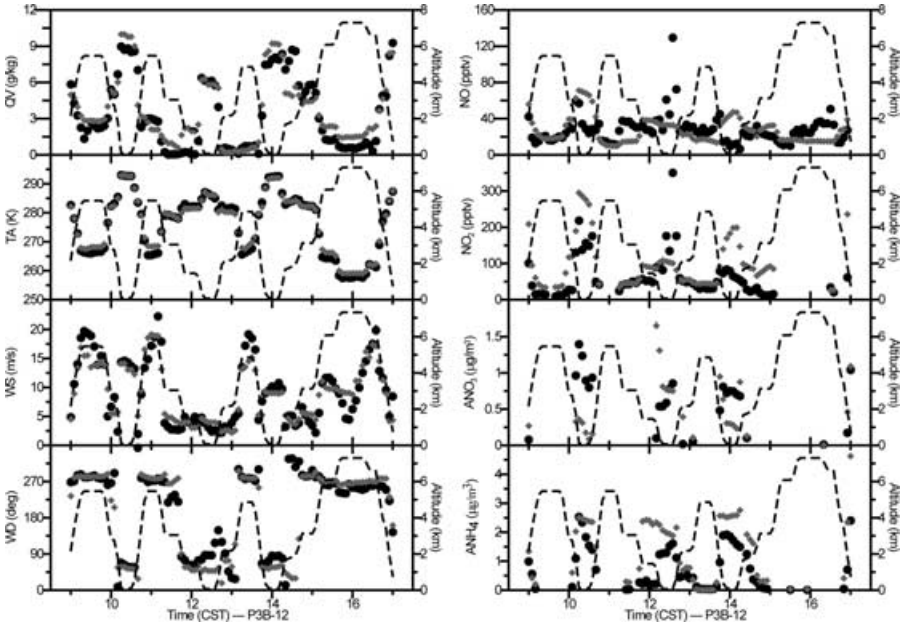

Fig. 3. Time series of observed (black dots) and simulated (grey diamonds) values of (a) specific humidity, (b) temperature, (c) wind speed, (d) wind direction, (e) NO, (f) NO_2, (g) ANO_3, and (h) ANH_4 along the track of the P3B flight 12 (dashed line, km) conducted on 13 March 2001. Units are g/kg, K, m/s, degree, pptv, pptv, $\mu g/m^{-3}$, and $\mu g/m^{-3}$, respectively.

Figures 3–6 show time series of observed and simulated values of specific humidity (QV), temperature (TA), wind speed (WS) and wind direction (WD) and concentrations of NO, NO_2, ANO_3 and ammonia aerosol (ANH_4) along the tracks of P-3B flight 12–15. On 13 March, the P-3B took off at about 0900 CST (Chinese Standard Time), i.e., 0100 UTC, from Hong Kong, and firstly headed south eastward and eastward, and then took a track heading north to the east of Taiwan along 124.5°E. After about 1230 CST it flew back to Hong Kong with a short leg of high altitude sampling into the South China Sea planned to look for potential biomass outflow (*cf.* Figs. 2a and 3e–h). The observed meteorological parameters displayed in Figs. 3a–d show that specific humidity and air temperature decreased with height while wind speed increased, and westerly winds prevailed in the

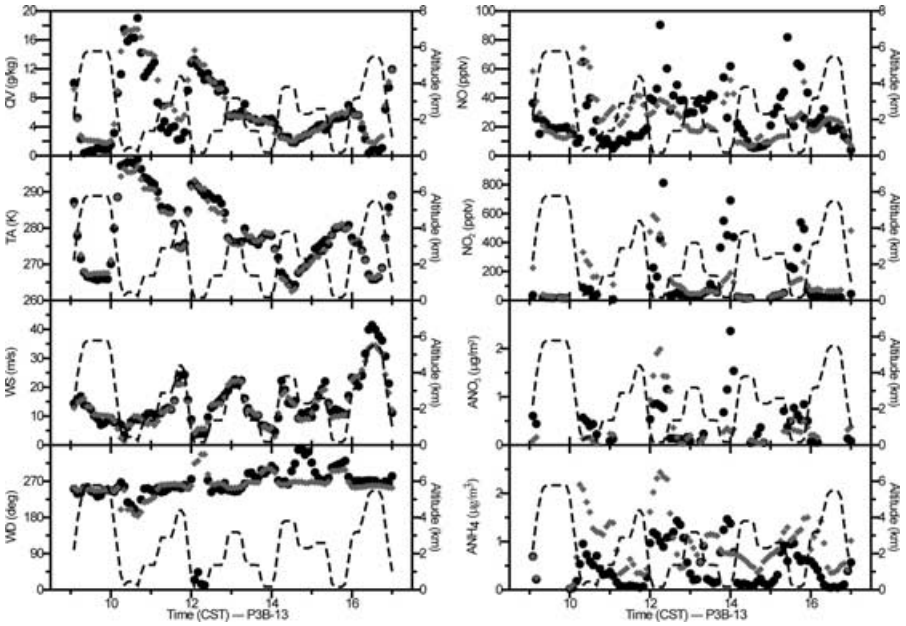

Fig. 4. Same as in Fig 3 but for the P3B flight 13 on 17 March 2001.

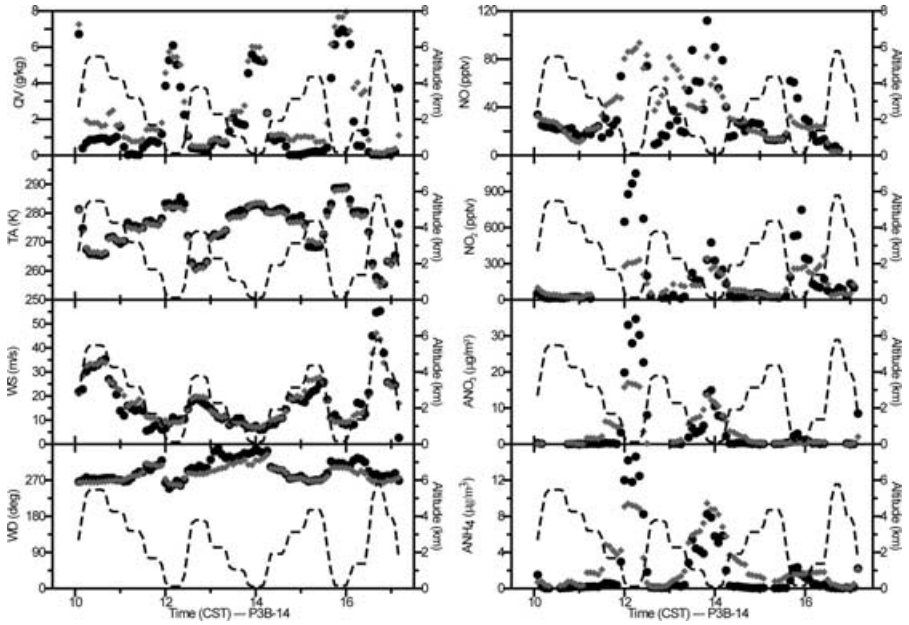

Fig. 5. Same as in Fig 3 but for the P3B flight 14 on 18 March 2001.

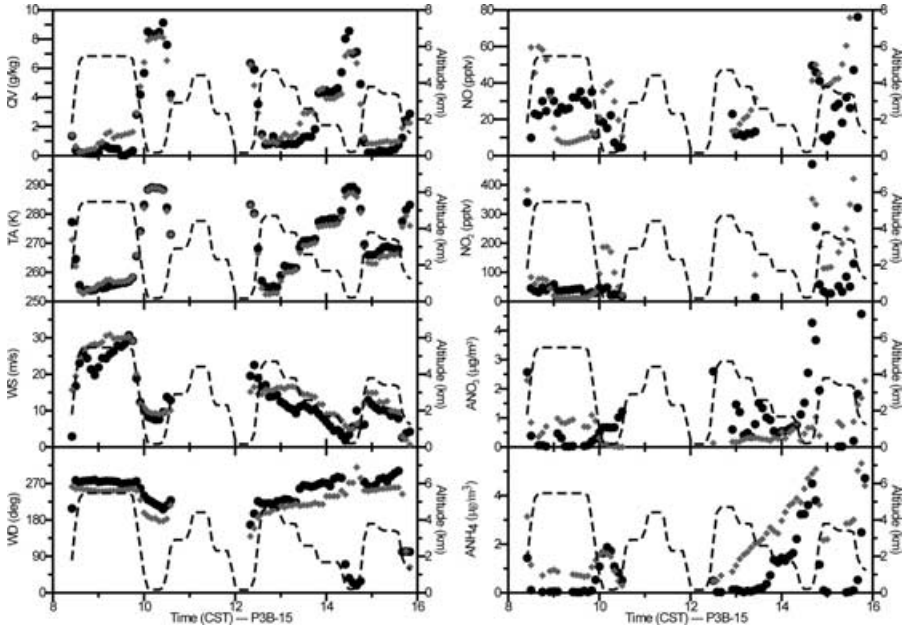

Fig. 6. Same as in Fig 3 but for the P3B flight 15 on 21 March 2001.

layers above ∼4 km while wind directions in the lower atmosphere changed from north-easterly in the area to the south of Taiwan (∼1030 CST) to south-easterly over the East China Sea (∼1230 CST). From Figs. 3a–d we find that the modelled values of specific humidity, temperature, wind speed and wind direction are generally in good agreement with the observed ones.

Figures 3e–h show that the measured NO, NO_2, ANO_3 and ANH_4 concentrations exhibited large variations in time and space: for example, their values were generally high in the lower troposphere and usually low at upper layers, but differed sometimes greatly even at the same height. From these figures we find that the modelled values agree reasonably well with their observed ones, and the model captured their variations in time and space well, e.g., high concentrations of NO, NO_2 and ANH_4 over the water area to the south of Taiwan (∼1030 CST) were well reproduced. Preliminary analysis of model results indicates that these high concentrations might be associated with pollution outflow from Taiwan as north-easterly winds were simulated

over the area (*cf.* Fig. 3d). Figures 3e–f also show that the model could not capture very high levels of NO and NO_2. Underestimation of maximum NO and NO_2 values may be primarily due to the coarse grid resolution and uncertainties in the emissions used in this study.

The P-3B started observations at about 0900 CST from Hong Kong on 17 March. It firstly flew south-eastward and then north-eastward to (22°N, 124.5°E), turned north at this point into the Yellow Sea along 124.5°E up to 37°N, and finally returned south into Okinawa. Figures 4a–d show that specific humidity and temperature in the lower atmosphere were higher at low latitudes (∼1030 CST) than at mid-latitudes (∼1400 and 1540 CST), winds were predominantly westerly in the layers above ∼4 km and south-easterly in the low atmosphere at low latitude (∼1030 CST) while north-westerly at mid-latitude (∼1540 CST), and wind speeds at high altitudes were larger at mid-latitudes than at low latitudes. As shown in these figures, these observed features are all well reproduced by the model.

Figure 4d shows that prevailing winds were north-westerly in the lower atmosphere and at mid-latitude, so mixing ratios of many chemical species over there were under direct influences of the emissions over the continental boundary layer. From Figs. 4e–f we find quite high values of NO and NO_2 in the lower troposphere at mid-latitudes and their concentrations were generally higher than those at low latitudes monitored during the previous flight (*cf.* Figs. 3e–f), and these observed features are also well captured by the model.

On 18 March, the P-3B conducted observations mainly over the East China Sea and the Yellow Sea. This flight between Okinawa and Yokota, an airbase near Tokyo (*cf.* Fig. 2c), was planned to include a northbound leg along 124.5°E beginning at 30°N stretching into the Yellow Sea up to 37°N, then south again before heading east toward Yokota. Figures 5a–d show that specific humidity was low and north-westerly winds prevailed in the lower troposphere. Under such conditions very high concentrations of NO, NO_2, ANO_3 and ANH_4 as shown in Figs. 5e–h were observed at ∼1210 and 1400 CST over the East China Sea and the Yellow Sea. Concentrations of ANO_3 and ANH_4 were much higher comparing with those obtained during the flights conducted on 13 and 17 March (*cf.* Figs. 3g–h and Figs. 4g–h). From Fig. 5 we can see that the model results are generally in good agreement with the observations.

The flight of the P-3B to the east of Japan was conducted on 21 March. It started observations at about 0830 CST, and firstly headed south-eastward and then eastward, turned north and flew along 150°E, finally returned to Yokota (*cf.* Fig. 2d). Figures 6f–h show that high levels of NO_2, ANO_3 and ANH_4 were observed at ∼1430 CST and in the region close to Tokyo, and the model reproduced these high values quite well while ANO_3 was greatly underestimated at ∼1430 CST. From Fig. 6 we find that modelled meteorological parameters and chemical species are generally in good agreement with their observed ones except for wind directions and ANO_3 at ∼1430 CST. The observed winds were north-easterly while the simulated were north-westerly, which might lead to the great underestimation of ANO_3.

Table 1. Statistical summaries of model results and the observations along the P-3B flights 12–15.

	QV[c]	TA[b]	WS[a]	WD[a]	NO[b]	NO_2[b]	ANO_3[b]	ANH_4[b]
N[c]	349	349	349	349	316	244	190	280
C_O[d]	3.52	275.3	13.35	247.5	35.7	117.0	2.00	1.05
C_M[d]	3.99	274.8	13.72	240.9	30.5	122.3	1.63	1.79
σ_O[d]	3.63	10.5	8.57	75.7	54.0	214.6	5.38	2.07
σ_M[d]	3.57	10.1	8.06	71.0	21.8	135.7	3.32	1.88
R[e]	0.96	0.99	0.94	0.66	0.48	0.44	0.82	0.83

[a]QV, TA, WS, and WD represent for wind speed (m/s), wind direction (°), temperature (°K) and specific humidity.
[b]Units of NO, NO_2, ANO_3 and ANH_4 are pptv, pptv, $\mu g/m^{-3}$ and $\mu g/m^{-3}$, recpectively.
[c]N is the number of paired samples.
[d]C_O, σ_O, C_M and σ_M are the average value and the standart deviation of observed and modeled quantities.
[d]R stands for the correlation coefficient between observed and modeled quantities.

The above analysis and the statistics summaries presented in Table 1 show that meteorological parameters exhibited strong variations in time and space over East Asia, for example, horizontal wind speed and direction changed significantly in the lower atmosphere, while westerly winds prevailed in the layers above ∼4 km and winds were much stronger at mid-latitudes than at low latitudes (*cf.* Figs. 3c–d and 4c–d), and as shown in Table 1, the standard deviation (*SD*) of specific humidity (3.63 g/kg) is comparable to its average value (3.53 g/kg), and the standard deviations of wind speed and wind direction are as large as 8.57 m/s and 75.73°. From Fig. 3–6 and Table 1 we can see that the model reproduced the time spatial variations in specific humidity, temperature, wind speed and direction quite well, the average values of the modelled parameters are all in good agreement with their observed ones. The correlation coefficients between model results and observations are 0.96, 0.99, 0.94 and 0.66, respectively. Although the correlation coefficient for wind directions is relatively low, the percentage of the comparison points at which the absolute bias is within 30° is 79.9% if we use a value of 30° as the desired accuracy criteria for wind directions (Cox et al., 1998). As the observations used in this study were obtained over the western Pacific, further evaluation of the model's ability in producing local circulation and boundary structure over urban areas and mountainous regions needs to be done.

Fig. 3–6 also show that the concentrations of NO, NO_2, ANO_3 and ANH_4 have strong tempo-spatial variations with high values in the lower troposphere. That is because NOx and NH_3 are mostly emitted in the continental boundary layer, and NO, NO_2, ANO_3 and ANH_4 levels over the water areas strongly depend on the transport and transformation processes. Comparing the

observed concentrations in the layers below ∼2 km on different days and over different areas, we find that NO_2 concentrations were generally much higher over the Yellow Sea and the East China Sea on 17 and 18 March (*cf.* Figs. 3f and 4f) than over the South China Sea on 13 March (*cf.* Fig. 2f), and the mixing ratios of ANO_3 and ANH_4 on 18 March (*cf.* Figs. 4g–h) greatly exceeded those on 17 March (*cf.* Figs. 3g–h) over the Yellow Sea and the East China with nearly the same NO and NO_2 levels. From these figures we also find that the model captured these observed features well. Table 1 indicates that average simulated values of NO, NO_2, ANO_3 and ANH_4 generally agree with their observed ones, and correlation coefficients for ANO_3 and ANH_4 are larger than 0.80, while simulated standard deviations are much smaller than observed ones and correlation coefficients for NO and NO_2 are 0.48 and 0.44. The model's inability to reproduce very high levels of NO and NO_2 maybe due to the coarse resolution of the model system and missing NOx emissions, and this inability may lead to the underestimation of maximum ANO_3 and ANH_4 concentrations and low correlation coefficients for NO and NO_2.

3.2. *Geographical and seasonal distributions of ANO_Λ concentrations*

Figure 7 shows the geographical distributions of ANO_3 mixing ratios in East Asia in January, April, July and October in the boundary layer (approximately 0∼1000 m) as calculated by CMAQ. Results are presented as monthly averages. The ANO_3 concentrations have noticeable differences between the four months. Generally the concentrations are higher in the winter, spring and fall, and lower in the summer and seasonal variations are typically strongest over China. As nitrate aerosols in the model normally present as particulate ammonium nitrate (NH4NO3), formed from the reversible reaction of gas phase ammonia (NH3) and nitric acid (HNO3), and HNO_3 is easily absorbed by rain water and cloud water, so the seasonal variation in ANO_3 concentrations is heavily influenced by the seasonal changes in precipitation and temperature.

Figure 7a shows that in January elevated ANO_3 concentrations ($\geq 2\ \mu g/m^{-3}$) are mainly found over eastern China and its coastal areas with maximum concentrations in an area over Central China between the Yangtze River and the Yellow River. This area is characterized by high emissions of NOx and NH_3 (Streets et al., 2003; Benkovitz et al., 1996). In the wintertime the photochemical activity is relatively weak, but HNO_3 is formed through heterogeneous reactions on the surface of aerosols (Schaap et al., 2003). January is under the influence of the winter monsoon in East Asia due to strong pressure gradients between the Siberian (Continental) High and Okhotsk (Maritime) Low, and the precipitation is very low over China but is substantial over Japan. During the peak of the monsoon, there is strong subsidence in the major part of the East Asia continent (Ding, 1994), and

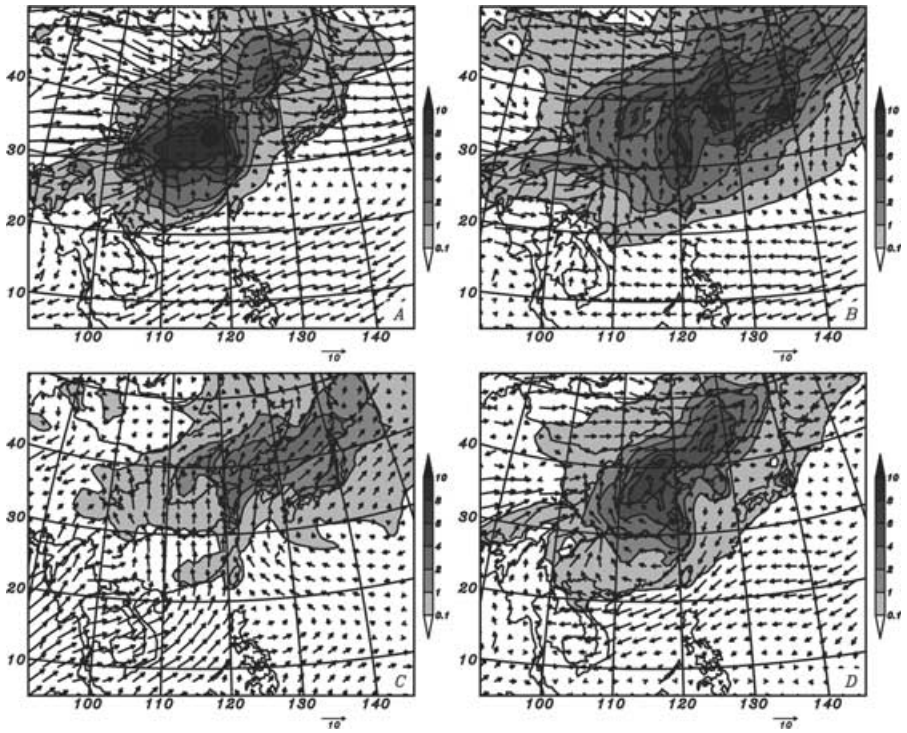

Fig. 7. Horizontal distributions of monthly averaged ANO_3 concentrations ($\mu g/m^3$) in the boundary layer (from surface to ∼1000 m) in (a) January, (b) April, (c) July and (d) October of 2001. Also shown are monthly averaged wind vectors at an altitude of ∼500 m.

pollution is trapped in the boundary layer. The monthly averaged wind flow pattern shown in Fig. 7a presents the typical pollutant transport pathway in association with the continental anticyclones and cold air outbreaks.

Spring in East Asia corresponds to the period of transition between the winter and summer monsoons (Ding, 1994), and strong north-westerly continental outflow occurs in April in the mid and upper troposphere. By March the Siberian High weakens, while the Pacific high-pressure system is building up. As a result, the strength of the winter monsoon winds and the frequency of occurrence of the cold south moving surges decrease, while incursions of warmer and tropical air from the south become frequent. As shown in Fig. 7b, the flow in the boundary layer is onshore over China south of about 30°N but strong westerlies prevail north of 40°N. The convergence zone over central and eastern China, where air masses from the north driven by monsoon winds encounter oceanic air masses from the south, plays an important role in the springtime export of pollution from the Asian continent (Zhang et al., 2003). Figure 7b shows a wide area with ANO_3 concentrations larger than 2 $\mu g/m^{-3}$ covering eastern China, Korea peninsula and Japan and part of the Yellow Sea and the Sea of Japan, and the transport processes played an important role in leading high concentrations over the region including the Yellow Sea and the Sea of Japan, and the water areas to the north-east of Japan. High levels of ANO_3 ($\geq$2 $\mu g/m^{-3}$) also attribute to stronger photochemical activity than in January.

July is in the middle of the summer monsoon season, westerly winds weaken and southerly monsoons dominate as far north as 30°N. The meteorological situation is characterized by predominant low level southerly and south-westerly circulation and a maximum in precipitation and cloudiness. The southerly winds push pollution northwards and north-eastwards. In the summer strong solar radiation leads to much more convection in the surface layer and increase of dry deposition of ANO_3. Model results show that the distribution pattern of dry deposition is quite similar to that of monthly averaged airborne concentration in the boundary layer presented in Fig. 7, and deposition amount increases from January to July. Figure 7c shows that the maximum concentrations are below $\sim$4 $\mu g/m^{-3}$ due to the higher cloud water contents, precipitation and temperatures and stronger dry deposition in July than in January.

October is in the early stage of the dry season over East Asia, and strong north-westerly continental outflow occurs in the mid and upper troposphere. Figure 7d shows anticyclone circulations over central and eastern China and prevailing westerlies and south-westerlies north of 40°N. The anticyclone circulations imply that much of the pollution originating in central and eastern China will flow clockwise out to sea then return to the south-west. While the westerly and south-westerly winds north of 40°N sweep pollution north-eastward. From Fig. 7d we can see that high ANO_3 concentrations ($\geq$2 $\mu g/m^{-3}$) are found over eastern China and its coastal areas north of 30°N. The general distribution pattern shown in Fig. 7d is similar to that in January, but maximum concentrations are smaller (*cf.* Fig. 7a) because of the subsidence over the continent is stronger in January in association with the winter monsoon.

4. Summary

The geographical and seasonal characteristics of nitrate aerosol concentration distributions in the boundary layer over East Asia in the year of 2001 were investigated by use of CMAQ with meteorological fields from RAMS. For evaluating the model performances, the modelled values of wind direction, wind speed, temperature and specific humidity and concentrations of NO, NO_2, ANO_3 and ANH_4 were compared with the observations obtained onboard the P3-B in the period 13 to 21 March 2001, when the P-3B performed four consecutive flights over four different regions: the South China Sea, the East China Sea, the Yellow Sea and the water areas to the east of Japan. Comparison shows that the observed wind direction, wind speed, temperature and specific humidity exhibited strong time spatial variations and the model captured these features. The modelled values are generally in good agreement with the observed ones, and the correlation coefficients are 0.66, 0.94, 0.99 and 0.96, respectively. If a value of 30° is used as the desired accuracy criteria for wind directions, the percentage of the comparison points at which the absolute bias is within the criteria reaches 79.9%. As the observations used in this study were obtained over the western Pacific, further evaluation of the model's ability in producing local circulation and boundary structure over urban areas and mountainous regions needs to be done.

The observations indicate that the mixing ratios of NO, NO_2, ANO_3 and ANH_4 strongly depended on their transport and transformation processes, and large concentrations were mostly detected in the layers below $\sim$2 km. The comparison shows that the model generally reproduced the concentration variation patterns along the flight tracks. The simulated average values agreed reasonably well with their observed ones, and correlation coefficients for ANO_3 and ANH_4 are larger than 0.80, while simulated standard deviations are much smaller than observed ones and correlation coefficients for NO and NO_2 are 0.48 and 0.44. Analysis indicates that the model was unable to reproduce very high levels of NO and NO_2 due to the coarse resolution of the model system and missing NOx emissions, and this inability may lead to the underestimation of maximum ANO_3 and ANH_4 concentrations and low correlation coefficients for NO and NO_2.

Analysis of horizontal distributions of monthly averaged ANO_3 concentrations in the boundary layer in January, April, July and October of 2001 shows that the ANO_3 mixing ratios have noticeable differences between the four months. Generally the concentrations are higher in the winter, the spring and the fall and low in the summer, and seasonal variations are typically strongest over China. Beside high emissions in NOx and NH_3, the maximum concentrations over central and eastern China in

January are due to the strong subsidence associated with the winter monsoon. Long-range transport may cause elevated concentrations in remote areas under favourable meteorological conditions, but the seasonal variation in the ANO_3 concentration is heavily influenced by the seasonal changes in precipitation and temperature.

5. Acknowledgments

This study was supported by grants from the Ministry of Science and Technology of China (Grant No. 2007CB407303 and 2005CB422205) and the National Natural Science Foundation of China (Grant No. 40333029). The authors gratefully acknowledge the team members of TRACE-P for the observational data.

References

AQEG (Air Quality Expert Group), 2005. Particulate Matter in the United Kingdom. Department of Environment, Food and Rural Affairs (DEFRA), London, UK. pp. 444 (available on-line at: http://www.defra.gov.uk/environment/airquality/aqeg).

Benkovitz, C. M., Schultz, M. T., Pacyna, J., Tarrason, L., Dignon, J., Voldner, E. C., Spiro, P. A., Logan, J. A. and Graedel, T. E. 1996. Global gridded inventories of anthropogenic emissions of sulfur and nitrogen. *J. Geophys. Res.* **101**, 29239–29253.

Binkowski, F. S. and Shankar, U. 1995. The regional particulate matter model: 1. Model description and preliminary results. *J. Geophys. Res.* **100**, 26191–26209.

Byun, D. W. and Ching, J. K. S. 1999. *Science algorithms of the EPA Models-3 community multi-scale air quality (CMAQ) modeling system*. NERL, Research Triangle Park, NC.

Cox, R., Bauer, B. L. and Smith, T. 1998. A mesoscale model intercomparison. *Bulletin American Meteorol. Soc.* **79**, 265–283.

Dentener, F. J. and Crutzen, P. J. 1993. Reaction of N_2O_5 on tropospheric aerosols: Impact on the global distributions of NO_x, O_3, and OH. *J. Geophys. Res.* **98**, 7149–7163

Ding, Y. 1994. The winter monsoon in East Asia. Chapter 2 in *Monsoons Over China*. Kluwer Academic Publishers, Dordrecht, 91–173.

Han, Z., Ueda, H. and Matsuda, K. 2005. Model study of the impact of biogenic emission on regional ozone and the effectiveness of emission reduction scenarios over eastern China. *Tellus* **57B**, 12–27.

IPCC (International Panel of Climate Change), 2001. *Climate Change 2001: The Scientific Basis*. Cambridge University Press, New York.

Jacob, D. J., Crawford, J. H. and co-authors. 2003. Transport and Chemical Evolution over the Pacific (TRACE-P) aircraft mission: Design, execution, and first results. *J. Geophys. Res.* **108**(D20), 9000, doi:10.1029/2002JD003276.

Kato, N. and Akimoto, H. 1992. Anthropogenic emissions of SO_2 and NO_x in Asia: Emission inventories. *Atmos. Environ.* **26A**, 2997–3017.

Kim, J. and Cho, S.-Y. 2003. A numerical simulation of present and future acid deposition in North East Asia using a comprehensive acid deposition model. *Atmos. Environ.* **37**, 3375–3383.

Kim, Y. P., Seinfeld, J. H. and Saxena, P. 1993. Atmospheric gas–aerosol equilibrium: Thermodynamic model. *Aerosol. Sci. Technol.* **19**, 157–181.

Mozurkewich, M. 1993. The dissociation constant of ammonium nitrate and its dependence on temperature, relative humidity, and particle size. *Atmos. Environ.* **27A**, 261–270.

Olivier, J. G. J., Bouwman, A. F., Van der Maas, C. W. M., Berdowski, J. J. M., Veldt, C. and co-authors. 1996. Description of EDGAR Version 2.0: A set of global emission inventories of greenhouse gases and ozone-depleting substances for all anthropogenic and most natural sources on a per country basis and on $1^\circ \times 1^\circ$ grid, Report no. 771060 002. National Institute of Public Health and the Environment (RIVM), Bilthoven, Netherlands.

Pielke, R. A., Cotton, W. R., Walko, R. L., Tremback, C. J., Lyons, W. A. and co-authors. 1992. A comprehensive meteorological modeling system – RAMS. *Meteorol. Atmos. Phys.* **49**, 69–91.

Schaap, M., Muller, K. and ten Brink, H. M. 2002. Constructing the European aerosol nitrate concentration field from quality analysed data. *Atmos. Environ.* **36**(8), 1323–1335.

Schaap, M., van Loon, M., ten Brink, H. M., Dentener, F. J. and Builtjes, P. J. H. 2003. The nitrate aerosol field over Europe: simulations with an atmospheric chemistry-transport model of intermediate complexity. *Atmos. Chem. Phys. Discuss.* **3**, 5919–5976.

Stockwell, W. R., Middleton, P., Chang, J. S. and Tang, X. 1990. The second generation regional acid deposition model chemical mechanism for regional air quality modeling. *J. Geophys. Res.* **95**, 16343–16367.

Streets, D. G. and Waldhoff, S. T. 2000. Present and future emissions of air pollutants in China: SO_2, NO_x and CO. *Atmos. Environ.* **34**, 363–374.

Streets, D. G., Bond, T. C., Carmichael, G. R., Fermandes, S., Fu, Q. and co-authors. 2003. An inventory of gaseous and primary aerosol emissions in Asia in the year 2000. *J. Geophys. Res.* **108**(D21), 8809, doi:10.1029/2002JD003093.

Turnbull, A. B. and Harrison, R. M. 2000. Major component contributions to PM10 composition in the UK atmosphere. *Atmos. Environ.* **34**, 3129–3137.

Van Aardenne, J. A., Carmichael, G. R., Levy II, H., Streets, D. and Hordjik, L. 1999. Anthropogenic NO_x emissions in Asia in the period 1990–2020. *Atmos. Environ.* **33**, 633–646.

Xie, M. 2002. The basic feature research of acid rain pollution in Guangzhou area between 1996 and 2000. *Res. Environ. Sci.* **15**(1), 31–33. (in Chinese)

Yu, R., Su, Y. and Li, Z. 2003. Analysis of feature of acid rain pollution and its formation cause in Fuzhou. *Fujian Geography* **18**(2), 23–25. (in Chinese)

Zhang, M., Uno, I., Zhang, R., Han, Z., Wang, Z. and Pu, Y. 2006. Evaluation of the Models-3 Community Multi-scale Air Quality (CMAQ) modeling system with observations obtained during the TRACE-P experiment: Comparison of ozone and its related species. *Atmos. Environ.* **40**(26), 4874–4882.

Zhang, M., Uno, I., Carmichael, G. R., Akimoto, H., Wang, Z. and co-authors. 2003. Large-scale structure of trace gas and aerosol distributions over the western Pacific Ocean during TRACE-P. *J. Geophys. Res.* **108**(D21), 8820, doi:10.1029/2002JD002946.

Zhang, M., Uno, I., Yoshida, Y., Xu, Y., Wang, Z. and co-authors. 2004. Transport and Transformation of Sulfur compounds over East Asia during the TRACE-P and ACE-Asia Campaigns. *Atmos. Environ.* **38**(40), 6947–6959.